IEEE Access
Multidisciplinary | Rapid Review | Open Access Journal

Received 12 March 2024, accepted 26 March 2024, date of publication 5 April 2024, date of current version 12 April 2024.

Digital Object Identifier 10.1109/ACCESS.2024.3385437

RESEARCH ARTICLE

Reducing Force Ripples and Enhancing Reliability in LSRMs Through Modern Structure and Advanced Control Systems

SIAMAK MASOUDI[1], (Member, IEEE), LAZHAR BEN-BRAHIM[1], (Life Senior Member, IEEE), ADEL GASTLI[1], (Senior Member, IEEE), NASSER AL-EMADI[1], (Member, IEEE), AND MOHAMED DJEMAI[2,3], (Senior Member, IEEE)

[1]Department of Electrical Engineering, Qatar University, Doha, Qatar
[2]LAMIH, INSA HdF, UPHF, 59313 Valenciennes, France
[3]Quartz, ENSEA, 95000 Cergy, France

Corresponding author: Lazhar Ben-Brahim (brahim@qu.edu.qa)

This work was supported in part by Qatar University (QU) under Grant IRCC-2022-543, and in part by the Qatar National Library (Open Access Funding).

ABSTRACT Linear switched reluctance motors (LSRMs) are highly popular due to their simple and robust structure, affordable pricing, and ability to operate at high efficiency. However, a major drawback of these motors is the high ripple force. In this paper, a novel structure for a linear motor with an exceptionally lightweight rotor and a stator with separate poles is presented, making it suitable for use in electric train systems. The proposed system not only significantly reduces force fluctuations but also enables the distribution of force along the length of the moving vehicle, ensuring smooth motion. Moreover, the reliability of the system is enhanced, as the LSRM can continue its motion even in the presence of a fault in one of the phases. In applications with high speeds, the use of a fast controller seems essential, but conventional fast regulators often lack sufficient precision. To address this issue, a new control system is introduced, utilizing a new 12-vector voltage switching table and a current controller. Unlike conventional control methods, the phases firing angle in the proposed system is not fixed. As a result, acceptable performance at different speeds is achieved through an adaptive real-time turn-on position control.

INDEX TERMS Multi-stator linear switched reluctance motor, force distribution, reliability, adaptive phase turn-on, switching table, current control, 2D finite element analysis.

I. INTRODUCTION

LSRMs are a type of electric motor that operates based on the principle of reluctance. They offer several advantages. Firstly, they do not require permanent magnets, making them cost-effective and environmentally friendly. Additionally, LSRMs have a simple mechanical structure, which reduces complexity and enhances reliability. The absence of brushes and commutators eliminates the need for maintenance and reduces wear and tear. Moreover, LSRMs can achieve high force density and provide precise positioning capabilities, making them suitable for various applications, including electric trains and automation systems.

Some structures of linear switched reluctance motors have been discussed and compared in [1] and [2], providing insights into their potential applications. A modern LSRM suitable for railway systems has been presented in [3], which includes permanent magnets (PMs). The structure can produce high propulsion force density but PMs increase the cost significantly. In [4], the design and analysis of a segmental stator double-sided LSRM for railway systems has been discussed. To improve the force density, high-temperature superconducting windings have been used in a single-sided LSRM [5]. An innovative LSRM, including modular and

The associate editor coordinating the review of this manuscript and approving it for publication was Ton Duc Do.

crooked-tooth translator, has been presented in [6] which has high force density and low force ripple compared with conventional motors. To improve the force density, a thickened stator yoke LSRM with a multi-tooth mover has been developed [7]. Despite the motor's capability of generating acceptable force, its large volume hinders its suitability for long-duration applications such as railway systems. To obtain a higher average force and a lower force ripple, optimization of an LSRM using seeker optimization and genetic algorithms has been done [8].

To control a switched reluctance motor and minimize ripple, various techniques have been proposed in recent years. A high flexibility and simple predictive control strategy for an LSRM has been presented in [9]. Another prediction-based method has been discussed in [10]. The strength of this method is that it does not require complex calculations and precise motor information, making it highly useful in nonlinear systems such as SRMs. Due to magnetic saturation, the highly coupled magnetic circuits, and the complex torque-speed characteristics, SRMs have inherent non-linear dynamics, which complicate their analysis and control. Fuzzy logic and adaptive controllers have demonstrated the ability to overcome this challenge to a significant extent [11]. An approach to achieving stable sensor-less operation in the presence of unbalanced conditions has been introduced in [12]. The method involves a modified full-cycle inductance partition-based scheme for estimating the rotor position, combined with an adaptive capability to handle unbalanced inductance. Another interesting strategy for improving SRM performance is a time-efficient torque shaping method which has been discussed in [13]. The method employs an efficient and desirable linear space by utilizing a torque mapping technique between the linear space and the nonlinear space. A direct torque control strategy can prepare a fast response for a switched reluctance motor drive [14], [15]. The approach presented in [14] combines the improved linear active disturbance rejection control with the hybrid optimization algorithm. According to [16], a switching table used in the controller exhibits significant reductions in torque ripple and root-mean-square current of the phase winding in the single-winding bearing-less switched reluctance motor, compared to traditional control methods. To have better performance at low speeds, a predictive strategy has been introduced in [17], which is based on a finite-control-set model. A solution for reconstructing phase currents and enhancing the direct torque control strategy in a four-phase SRM drive has been presented in [18]. The proposed method utilizes a 16-sector partition approach and introduces a novel voltage vector selection process that detects zero-current regions in each phase. To reduce the ripple, a new control system with a switching table for a switched reluctance motor has been presented in [14] which includes 12 voltage vectors. The sectors are obtained based on the actual position of the rotor in the inductance profile.

A novel structure for a linear motor with a lightweight rotor and a stator featuring separate poles, specifically designed for electric train systems, has been presented in this work.

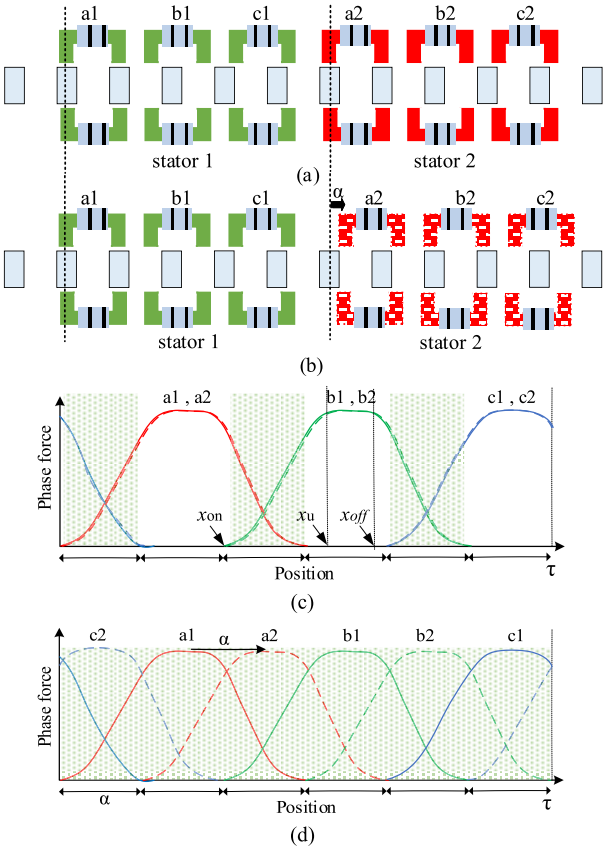

FIGURE 1. (a) Two stators without displacement, (b) two stators with displacement, (c) phase force of structure a, (d) phase force of structure b.

The proposed system significantly reduces force fluctuations, facilitates force distribution along the vehicle's length for smooth motion, enhances system reliability by allowing motion in the presence of a fault, and employs an adaptive real-time turn-on position control for optimal performance at different speeds.

In this work, the proposed LSRM and the proposed structure are presented in Section II. A comprehensive mathematical analysis of the proposed combination is performed in this section. The intended control system for the motor is presented in Section III. Finally, in Sections IV and V, the results obtained from simulation and practical experiments are demonstrated.

II. PROPOSED LSRM

A. MULTI-SECTION LSRM

The proposed motor focuses on the application of rail transportation systems. It has a simple translator without yoke and coils, making it suitable for use as a rail along the entire motion path. The three-phase LSRM with a double-sided stator configuration generates a high propulsion force while maintaining a zero normal force. In high-power applications, it is possible to use two or more similar stators side by side, as shown in Fig. 1 (a), which enhances the propulsion force. In the conventional structure, the stator sections are installed

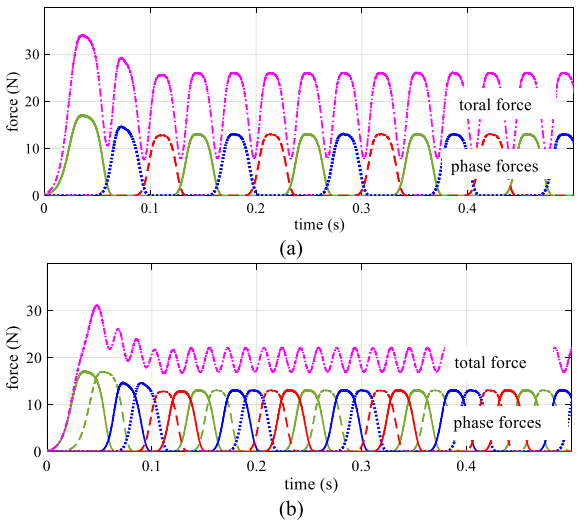

FIGURE 2. (a) Two stators without displacement, (b) two stators with $\alpha = \tau/6$ displacement.

in a similar spatial position relative to the translator, and the location of phase ''a'', which is aligned in both cases, is taken as the reference. Based on the phase forces shown in Fig. 1 (c), in most positions, two phases are on simultaneously, while during phase commutation, four phases are on together.

B. POLES ARRANGEMENT

Although control methods can improve the quality of the force, enhancing the performance can also be achieved through specialized motor design. In this work, considering the specific structure of the LSRM, an attempt is made to improve the quantity and quality of the force without changing the dimensions and characteristics of the motor, solely by adjusting the distance between the stator poles.

It has been suggested to install the stators with a deviation from the original stator configuration as shown in Fig. 1 (b). By displacing the stator poles relative to the translator, the phase force profile is also altered, as illustrated in Fig 1 (d). It can be observed that in all positions, three phases are simultaneously active, which is effective in both increasing the average force and reducing the ripple. The results of the simulations have shown that the best performance occurs when the side phases of the auxiliary stators cover the distance between the primary stator phases. Assuming τ as the translator pole-pitch for the three-phase (n = 3) LSRM, the deviation of the additional stators from the main stator is obtained as follows.

$$\alpha = \tau/k.n \tag{1}$$

where k denotes the total number of stators. For the proposed LSRM with dimensions shown in Table 3, $\tau = 70$ mm. A comparison of force in two conventional and proposed structure with $\alpha = \tau/6$ is shown in the Fig 2. Specifically, according to the figures, the conventional structures exhibit approximately 62% ripple in total propulsion force. With the introduction of $\alpha = \tau/6$ displacement, the ripple is significantly reduced to about 11%. This figure clearly demonstrates that the precise arrangement of stator poles can have a significant impact on reducing the force ripple.

C. VOLTAGE EQUATIONS

The control of a motor begins with a system model to properly regulate the system. Consequently, the system model must incorporate comprehensive and accurate information that represents the system's characteristics effectively. With the separate structure of the stator, mutual inductance can be neglected in the proposed LSRM. In this case, the voltage and flux linkage equations can be written as follows.

$$u_k = R_s i_k + \frac{d\lambda_k}{dt} \tag{2}$$

$$\lambda_k = L_k i_k \tag{3}$$

where u_k, i_k, and λ_k are phase voltage, phase current, and flux linkage for $k = a_1, a_2, b_1, b_2, c_1, and\ c_2$, respectively. R_s denotes a phase resistance. Assuming that at any given moment, three phases are active while the other three phases have zero current, (2) and (3) can be written as follows.

$$\begin{cases} u_1 = R_s i_1 + \dfrac{d\lambda_1}{dt} \\ u_2 = R_s i_2 + \dfrac{d\lambda_2}{dt} \\ u_3 = R_s i_3 + \dfrac{d\lambda_3}{dt} \end{cases} \tag{4}$$

$$\begin{cases} \lambda_1 = L_1 i_1 \\ \lambda_2 = L_2 i_2 \\ \lambda_3 = L_3 i_3 \end{cases} \tag{5}$$

where the numbers 1, 2, and 3 indicate the active phases. The phase voltages can be expressed as functions of the phase currents of the active phases. If the phase currents are chosen as state variables, differentiating (5) with respect to time yields,

$$\begin{cases} \dfrac{d\lambda_1}{dt} = L_1 \dfrac{di_1}{dt} + g_1 v.i_1 \\ \dfrac{d\lambda_2}{dt} = L_2 \dfrac{di_2}{dt} + g_2 v.i_2 \\ \dfrac{d\lambda_3}{dt} = L_3 \dfrac{di_3}{dt} + g_3 v.i_3 \end{cases} \tag{6}$$

where $v = dx/dt$ and $g_k = dL_k/dx$ denotes the rate of change of phase inductance with respect to position. By combining (6) and (4) and considering the phase currents as state variables, it can be written:

$$\begin{cases} \dfrac{di_1}{dt} = -\dfrac{R_s}{L_1} i_1 - \dfrac{g_1}{L_1} v.i_1 + \dfrac{1}{L_1} u_1 \\ \dfrac{di_2}{dt} = -\dfrac{R_s}{L_2} i_2 - \dfrac{g_2}{L_2} v.i_2 + \dfrac{1}{L_2} u_2 \\ \dfrac{di_3}{dt} = -\dfrac{R_s}{L_3} i_3 - \dfrac{g_3}{L_3} v.i_3 + \dfrac{1}{L_3} u_3 \end{cases} \tag{7}$$

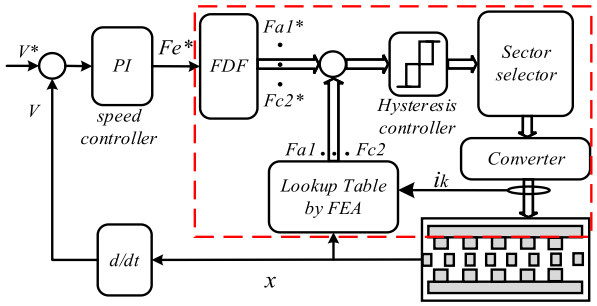

FIGURE 3. Block diagram of the controller including lookup table.

The resultant propulsion force is the sum of all phase forces, with three of them being active while the rest are off at any given moment.

$$F_e = F_1 + F_2 + F_3 = \frac{1}{2}g_1 i_1^2 + \frac{1}{2}g_2 i_2^2 + \frac{1}{2}g_3 i_3^2 \quad (8)$$

Also, the mechanical equation is expressed as follows.

$$F_e = \sum F_k = M\frac{d^2x}{dt^2} + C\frac{dx}{dt} + F_L \quad (9)$$

where, F_L is load force, and M and C are mass and friction coefficient, respectively.

D. CONVENTIONAL CONTROL SYSTEM

Due to the process of force generation, the control of LSRMs is more complex. The major issue with these motors is the presence of high ripple in the produced force, which limits their application. Besides optimizing the structure, the motor control system can also be designed in a way that reduces the level of ripple. In this section, the proposed motor control system is examined.

Direct force control (DFC) is a promising control method for linear SRMs, that uses a switching table for direct control of force and offering advantages in terms of simplicity, responsiveness, efficiency, and robustness, making it suitable for various industrial applications. Considering the absence of complex computations and the lack of PWM, which is time-consuming, this control method can be effective for the proposed motor. A block diagram of the control system in a LSRM is shown in Fig 3. In this structure, the FDF block represents the Force Distribution Function, responsible for allocating the commanded force value among different phases.

The controller exclusively applies hysteresis-loop control to instantaneous force and demonstrates a higher level of synergy with stator position signals in the proposed LSRM. It governs the switching states through the force hysteresis-loop. As shown in Fig. 3, a lookup table including data derived from finite element analysis has been utilized to find the phase force. Additionally, this approach does not involve time-consuming PWM. These lead to an exceptionally fast response in the control system.

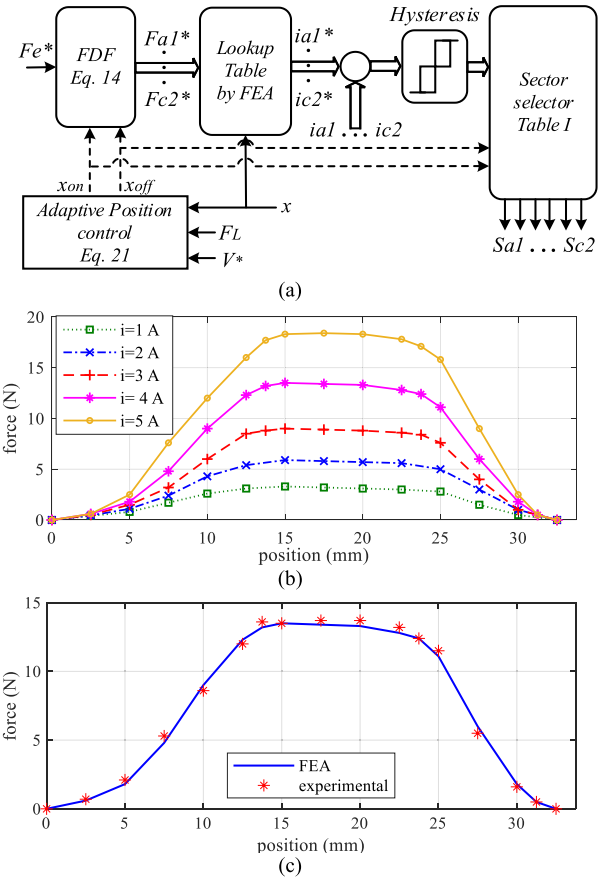

FIGURE 4. (a) Proposed control system, (b) force-position-current profiles, force obtained by FEA and experimental tests.

III. CONTROL OF LSRM

The main issue in control system shown in Fig. 3 is the generation of negative force and high force ripple, which are caused by the lack of current regulation. Moreover, it is inevitable that the fixed turn-on and turn-off angles will lead to negative force. To overcome the problems, a combined control method is proposed in this work, which includes a current controller without PWM. The proposed method involves two key modifications. Firstly, the hysteresis controller is applied to current instead of force. The results demonstrate that this approach significantly affects the force ripple magnitude. Secondly, an adaptive method is introduced to precisely calculate and regulate the turn-on position for each phase, providing self-tuning capabilities to the controller and enhancing its performance in different situations.

A. CURRENT REGULATION CAPABILITY

The proposed control system is illustrated in Fig. 4 (a). It can be seen that a hysteresis controller is employed to regulate the current of the phase. In this approach, the system does not become more complex since the reference current is determined solely by using a lookup table without the need for additional calculations. The lookup table contains finite element analysis data, which was used in the conventional method to determine the actual force.

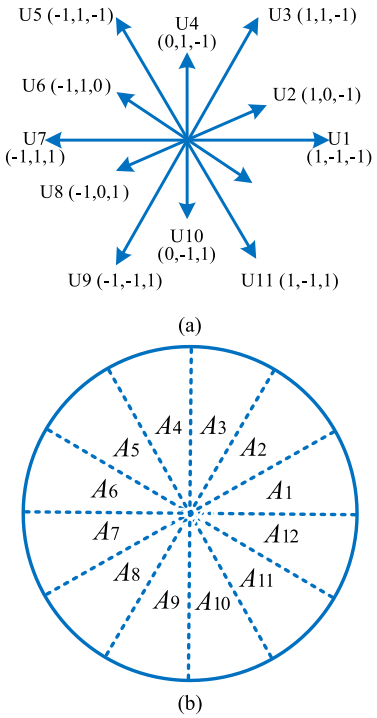

FIGURE 5. (a) Voltage vectors, (b) sectors by 12 voltage vectors.

TABLE 1. Voltage vector selection table.

voltages / sector	A_1	A_2	A_3	A_4	A_5	A_6
T_+	U_5	U_6	U_7	U_8	U_9	U_{10}
T_-	U_9	U_{10}	U_{11}	U_{12}	U_1	U_2
voltages / sector	A_7	A_8	A_9	A_{10}	A_{11}	A_{12}
T_+	U_{11}	U_{12}	U_1	U_2	U_3	U_4
T_-	U_3	U_4	U_5	U_6	U_7	U_8

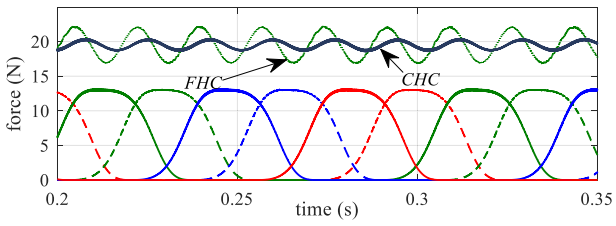

FIGURE 6. Comparison between force hysteresis control (FHC) and current hysteresis control (CHC) methods at $v = 0.5m/s$.

The lookup table of the proposed LSRM contains three-dimensional data obtained from finite element analysis (FEA), that illustrates the relationship between force, position, and current in a phase, as shown in Fig. 4 (b). The comparison of the phase force curves obtained from finite element analysis and practical testing for a current of 4 A is shown in Fig. 3 (c). The comparison of the values

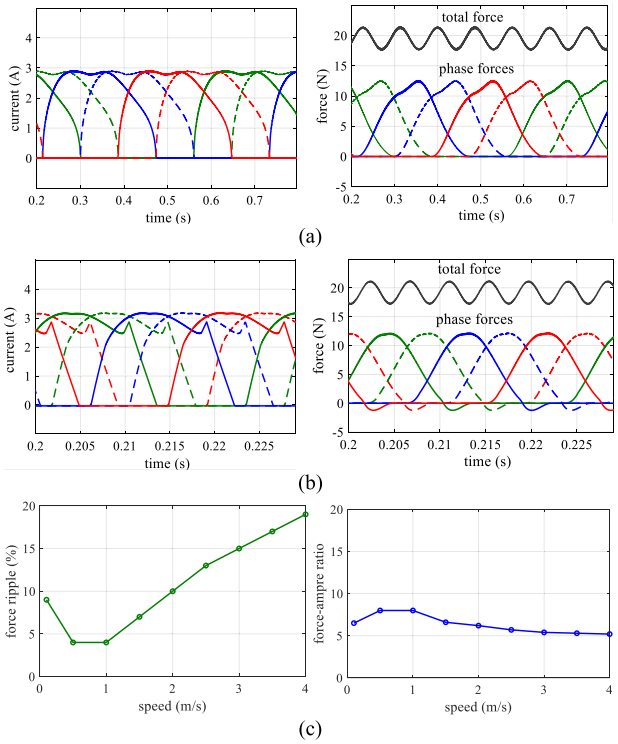

FIGURE 7. Proposed method at different speeds, (a) $v = 0.1m/s$, (b) $v = 2m/s$.

obtained from experimental results demonstrates that they are nearly identical to the FEA, with a very negligible difference between them.

To improve the performance quality of the hysteresis controller, new vectors and sectors have been defined based on the spatial positions of the poles [14]. For this purpose, the number of sectors has increased from 6 to 12, and correspondingly, 12 voltage vectors have been provided as Fig. 5.

The voltage vector selection rule is also presented in the TABLE 1.

By employing voltage vectors and sections, the propulsion force curve for two control systems indicated in Fig. 3 and Fig 4, is obtained as Fig 6. Comparing the two curves in each figure illustrates that controlling the phase currents can have a significant impact on the ripple of the force.

B. RUNAWAY PHENOMENON

In an LSRM, the force is produced by aligning the translator's salient poles with the stator poles through controlled switching of current in the motor windings. If the motor control system fails to correctly control the current switching or loses feedback from sensors, the motor can enter an undesired state, which is called the runaway phenomenon [19], [20]. It has an effect on the quantity and quality of the propulsion force. This phenomenon appears at low and high speeds as shown in Fig. 7. The average force over a cycle (F_{av}) and ripple factor (RF) are calculated using (10) – (13) and are illustrated in Fig. 7 (c). These results indicate that, an unchanged turn-on

position leads to ripple problem at high and low speeds.

$$F_{av} = \frac{1}{T_{sp}} \int_0^{T_{sp}} F_k\left(i_1, i_2, i_3, x\right) dx \tag{10}$$

$$F_{rms} = \sqrt{\frac{1}{T_{sp}} \int_0^{T_{sp}} F_k^2\left(i_1, i_2, i_3, x\right) dx} \tag{11}$$

$$F_{ac} = \sqrt{F_{rms}^2 - F_{av}^2} \tag{12}$$

$$RF = \frac{F_{ac}}{F_{av}} \tag{13}$$

where, F_{rms} is the effective force and F_{ac} is ac component of the propulsion force. Also, T_{sp}, F_t, and (i_1, i_2, i_3) denote the time period of one cycle, phase force, and on phases current, respectively. Thus, the force-ampere ratio can be expressed by $\sigma = F_{av}/i_{av}$.

C. ADAPTIVE PHASE TURN-ON

The issues mentioned in the previous section exist for all force distribution functions (FDFs). It means that fixing the phase turn-on leads to a decrease in system performance at both high and low speeds. In this section, an adaptive method is presented for adjusting the turn-on position, that is applicable to all functions. A quadratic function has been selected for distributing the power between the phases. The results obtained in the previous sections were also derived using this function.

$$f_k = \begin{cases} 0 & 0 \le x \le x_{on} \\ \frac{3}{x_{ov}^2}\left(x - x_{on}\right)^2 - \frac{2}{x_{ov}^3}\left(x - x_{on}\right)^3 & x_{on} \le x \le x_{on} + x_{ov} \\ 1 & x_{on} + x_{ov} \le x \le x_{off} \\ 1 - \frac{3}{x_{ov}^2}\left(x - x_{off} + x_{ov}\right)^2 - \frac{2}{x_{ov}^3}\left(x - x_{off} + x_{ov}\right)^3 & x_{off} \le x \le x_{off} + x_{ov} \\ 0 & x_{off} + x_{ov} \le x \le \tau \end{cases} \tag{14}$$

where, f_k denotes the force distribution function of phase k and x_{on}, x_u, x_{off}, and τ are shown in Fig. 1 for phase b. The reference value of a phase force (F_k^*) is obtained based on the total desired force (F_e^*) and FDF of the corresponding phase.

$$F_k^* = f_k.F_e^* \quad k = a_1, \ldots, c_2 \tag{15}$$

$$\sum_{a_1}^{c_2} f_k = 1 \tag{16}$$

In the conventional control system, using fixed values for x_{on} and x_{off} not only lead to an increase in the force ripple of the LSRM but also cause negative force generation, ultimately reducing the motor's efficiency. Therefore, it becomes crucial to carefully select the optimal x_{on} and x_{off} values corresponding to different operating speeds and load forces.

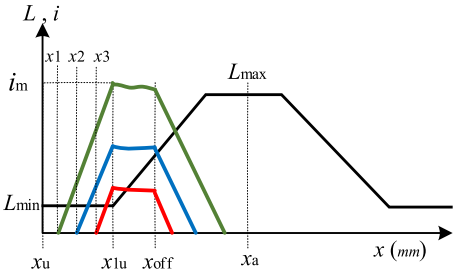

FIGURE 8. Phase inductance and currents vs stator position.

Usually, the relationship between x_{on} and x_{off} is determined based on (17), where τ and m denote the pole pitch of the moving part and the number of motor phases, which are 70 *mm* and 6 in the proposed LSRM, respectively.

$$x_{off} - x_{on} \le \tau/m \tag{17}$$

Fig. 8 indicates a phase current generated by three different turn-on positions. x_u, x_{1u}, and x_a are unaligned, overlapping, and aligned positions, respectively. It can be seen that the choice of the turn-on position (x_{on}) impacts the phase current behavior. A smaller position (x_1) leads to a quick current increase with a high peak (i_m). Opting for a moderated angle results in a steady current waveform with no significant i_m. However, a larger angle causes a gradual current rise, risking inadequate propulsion force production. Hence, determining the optimal x_{on} depends on varying speeds and load forces to achieve consistent force delivery.

In this section, an adaptive method has been proposed to optimally determine the turn-on position in the proposed LSRM drive. Ignoring the resistance voltage drop in (2), it is written as follows.

$$u_k = \frac{d\lambda_k}{dx} = \frac{d\lambda_k}{dx}.v \tag{18}$$

By integrating (18) over the interval from x_{on} to x_{1u}, it can be expressed as (19). The flux linkage and phase force are functions of the rotor position and phase current. Therefore, by knowing the force and position and utilizing the lookup table obtained by FEA, the phase current can be determined. Consequently, (18) can be rewritten as (19).

$$\lambda_k\left(x_{1u}\right) - \lambda_k(x_{on}) = \frac{U_k}{v}(x_{1u} - x_{on}) \tag{19}$$

$$\lambda_k\left(x_{1u}, i\left(x_{1u}, F_{1u}^*\right)\right) - \lambda_k\left(x_{on}, i\left(x_{on}, F_{on}^*\right)\right) = \frac{U_k}{v}(x_{1u} - x_{on}) \tag{20}$$

where F_{1u}^* denotes the reference force corresponding to x_{1u}. With an appropriate approximation, $\lambda_k\left(x_{on}, F_{on}^*\right)$ is zero, while $\lambda_k\left(x_{1u}, F_{1u}^*\right)$ is the flux linkage in position x_{1u} when the reference force is F_{1u}^*. So, the turn-on position can be calculated as follows.

$$x_{on} = x_{1u} - \frac{\lambda_k\left(x_{1u}, F_{1u}^*\right)}{U_k}.v \tag{21}$$

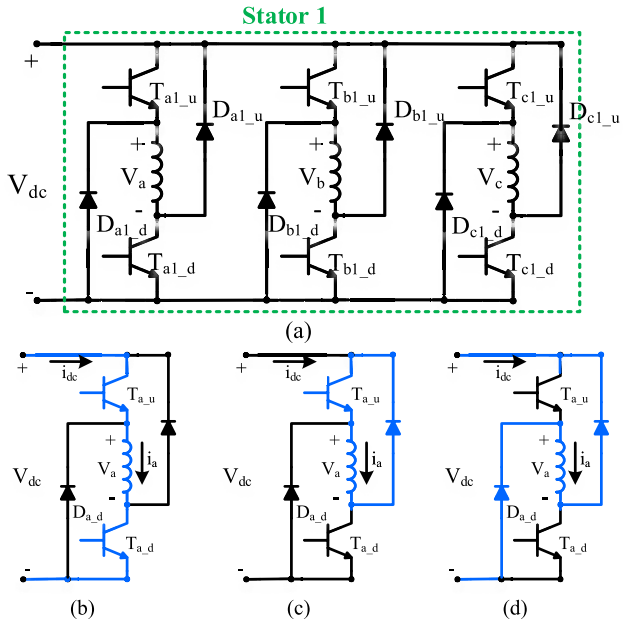

FIGURE 9. Asymmetric half bridge converter and operation modes.

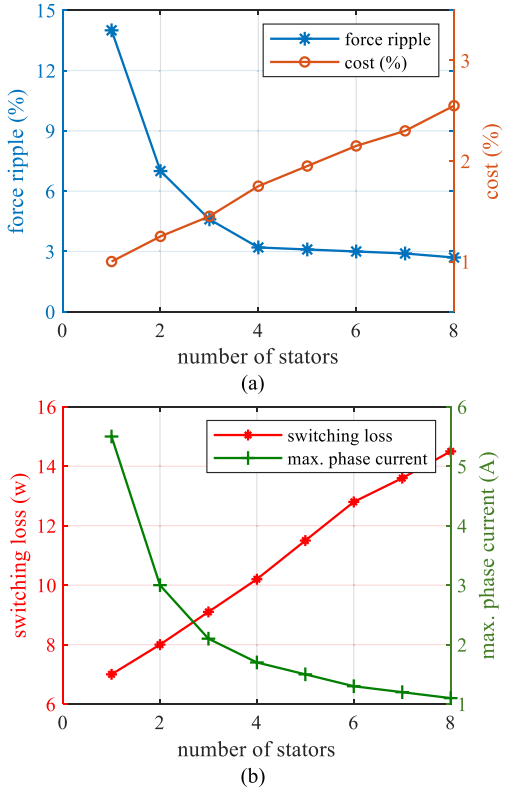

FIGURE 10. Performance comparison for various number of stators: (a) Force ripples, (b) switching losses.

D. ASYMMETRICAL HALF BRIDGE CONVERTER

Half-bridge converters, known for their simplicity and cost-effectiveness, boast low component stress, high efficiency, and precise modulation control. These attributes make them a suitable choice for controlling SRMs. The primary circuit of the utilized asymmetrical half-bridge (AHB) converter is depicted in Fig. 9. In this configuration, each phase features two switches, and there are three possible states for each phase winding within the AHB converter while phase current is present. The commutation process from phase A to phase B is illustrated in Fig 9 (b), (c), and (d). When both switches, T_{a_u} and T_{a_d}, are simultaneously activated, phase A becomes energized, causing a rise in current and subsequently increasing force. This state is denoted as "1". If one of the two switches is turned off, the circuit enters a freewheeling state, marked as "0". In this condition, neither the current nor the torque in phase A continues to increase or decrease. When both T_{a_u} and T_{a_d} switches are turned off, phase A undergoes demagnetization, resulting in a decrease in current and force. This state is marked as "-1". Concurrently, phase B commences its excitation as it prepares to take over the phase function.

IV. MULTI STATOR LSRM

In this work, it is proposed to use an LSRM with two similar stator parts which have spatial displacement from each other. As demonstrated in previous sections, this structure enhances the quality of the propulsive force and improves system efficiency. To better investigate this topic, a comparison has been made between different number of stators. The basis of these comparisons is for the proposed motor with a specified number of stators to ultimately generate a propulsive force of 20 N under no-load conditions. To simplify calculations and data extraction, with a suitable approximation, it is assumed that the slope of the phase inductance remains constant. Consequently, the main parameter in determining the force magnitude in each phase will be the current of that respective phase. Since all corresponding phases in different stators are turned on or off simultaneously, a single power converter can be used in accordance with the given configuration. However, the investigation revealed that this approach leads to disturbances. On the other hand, using an independent converter for each stator increases the system's reliability. Through numerical analysis, some parameters have been extracted and presented in Fig. 10. In accordance with the figure, as the number of stators increases, the ripple force decreases. This reduction is particularly significant up to four stators. The cost is also indicated in the same figure. In the cost calculation, the cost of the one-stator-motor has been taken as the baseline, and others have been expressed relative to it. 20% of the total cost includes components such as iron, wire, power electronic converters, etc., considered as manufacturing expenses. Additionally, according to Fig. 10, due to the decrease in the power of the stators, the phase current decreases. However, conversely, due to the use of more switches, switching losses increase. The results obtained indicate that a three-stator LSRM can have the best performance.

The structure of the proposed system including m stators is shown in Fig. 11 (a). The data have been obtained based on

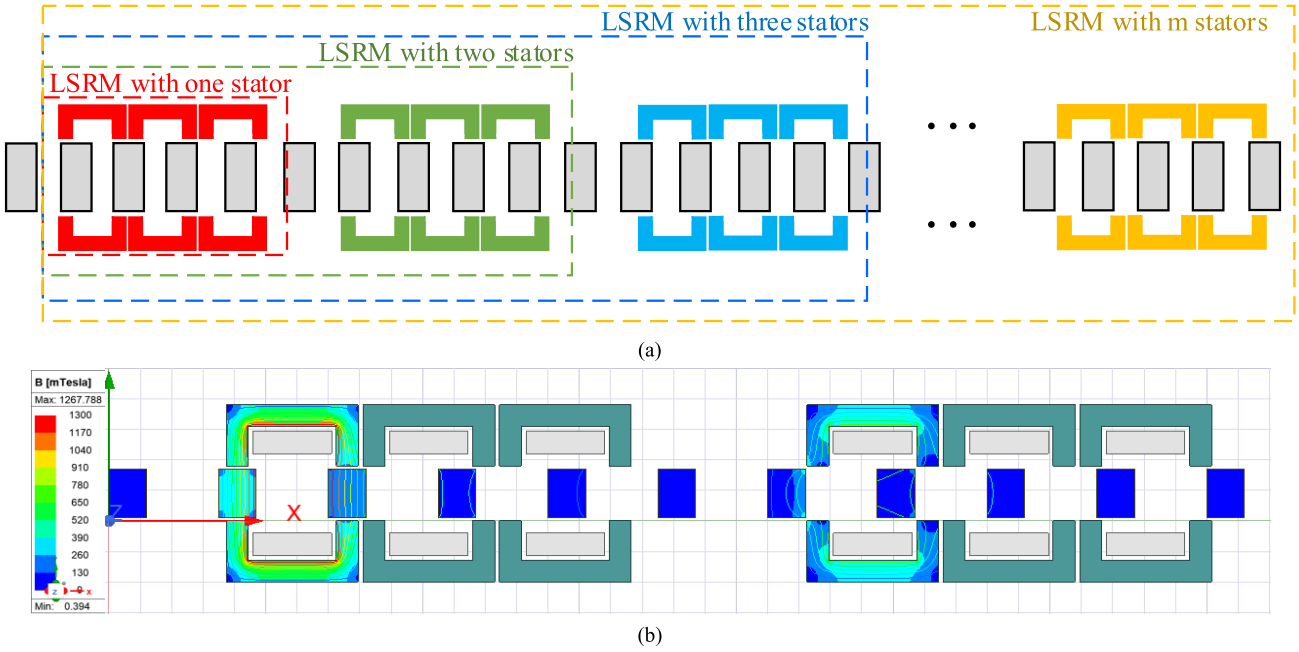

FIGURE 11. Proposed LSRM, (a) m-stator motor, (b) 2D finite element analysis of a LSRM with two stators.

TABLE 2. Dimensons of the LSRM with one stator.

variable	
Air gap length (mm)	2
Stator pole width (mm)	14
Stator slot width (mm)	56
Stator pole height (mm)	26
Translator pole width (mm)	24
Translator slot width (mm)	46
Translator pole height (mm)	32
Airgap between stator parts (mm)	3
Winding turns	150
Rated current (A)	3
Rated voltage (V)	100
Rated speed (m/s)	1
Coefficient of friction (C)	10
Phase resistance (Ω)	2.2

finite element analysis of different structures. 2D FEA of a LSRM including two stator sections are shown in Fig. 11 (b). Additionally, the calculation of converter power losses based on the difference between input and output power of the overall converters has been performed. Als, the deviation of the additional stators from the main stator is obtained as (1). TABLE 2 indicates that increasing the number of stators improves the quality of the generated force and enhances motor performance. It appears that the optimal choices are

TABLE 3. Numerical values for force profiles in Fig. 17.

variable	Method in [14]			Proposed method		
	Av. (N)	Max (N)	ripple	Av. (N)	Max (N)	ripple
0.5 m/s	19.2	20	5 %	19.6	19.9	3 %
2 m/s	19.4	20.3	8 %	19.6	20	3.6 %

2 or 3 stators since, in these cases, the ripple force reaches an acceptable level, and further increases do not significantly reduce it, while power losses and source current increase. Therefore, using multiple stators can improve force quality and enhance system reliability. In the event of a fault in one of the phases or windings, a malfunction does not occur in the motor's operation, allowing the motor to continue functioning seamlessly.

V. SIMULATION EVALUATION

To validate the proposed structure of the linear motor and control method, simulation and experimental tests were conducted using a LSRM prototype. The dimensions and parameters of the LSRM are outlined in TABLE 2. The performance of the proposed control system and the impact of the adaptive method on force quality are illustrated in Fig. 12. It can be observed that the drive system performs well at low and high speeds, 0.1 m/s and 2m/s, respectively. The phase current and inductance curves are also visible in Fig. 12(c).

By defining the parameters in Fig. 8 for one phase as $x_{on} = 35\,mm, x_u = 0, x_{1u} = 5\,mm$, and $x_{off} = x_{on} + \tau/m$, the turn-on positions at different speeds and loads have been obtained

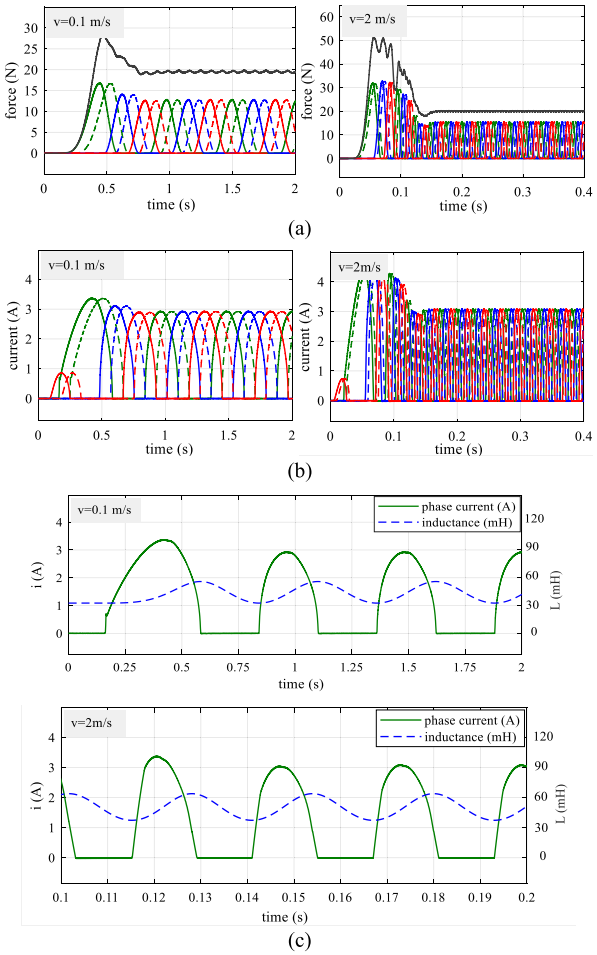

FIGURE 12. Performance of the proposed system, (a) total force and phase force, (b) current, (c) current and inductance.

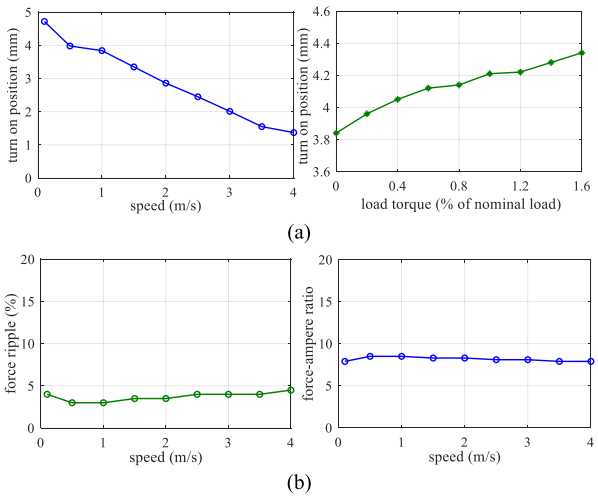

FIGURE 13. Comparison at different speeds and loads, (a) turn on position obtained by adaptive system, (b) force ripple and force ampere ratio.

using the adaptive method as illustrated in Fig. 13. Comparing this figure with the results shown in Fig. 7 indicates that the proposed method has a significant impact on reducing ripple levels and preventing force-ampere ratio reduction at

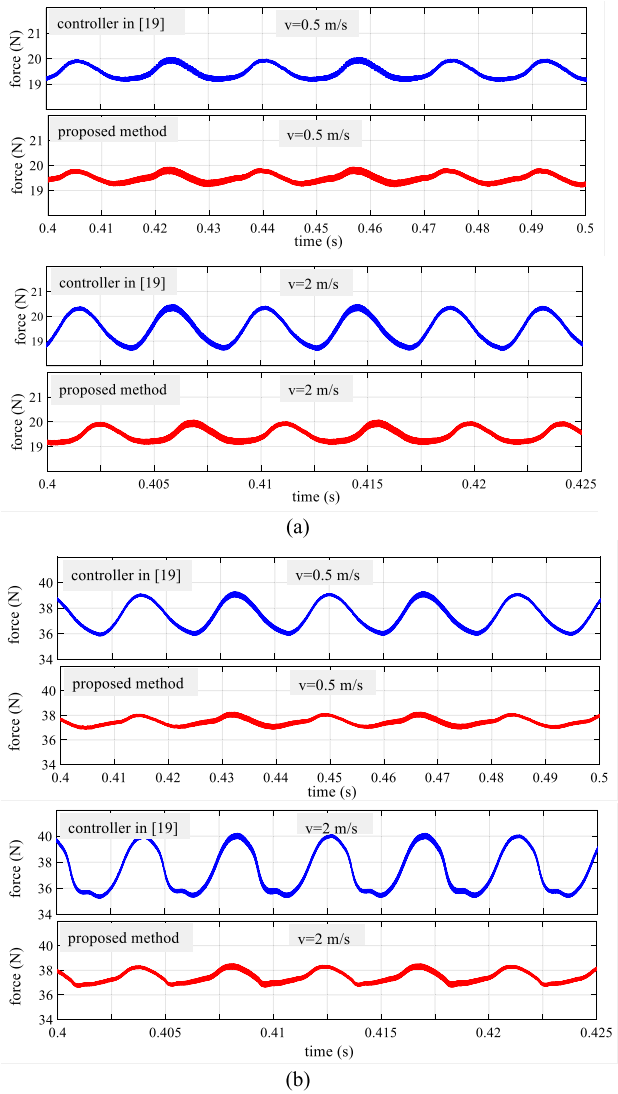

FIGURE 14. Comparison of force waveforms of the proposed system and the controller presented in [14], (a) no-load, (b) full-load condition.

high speeds. For further examination of the efficiency of the proposed control strategy in the proposed LSRM, its performance has been compared at two different speeds and under both no-load and full-load conditions with the modern controller presented in [14]. Based on these results, the two methods exhibit relatively similar performance at low speeds and under no-load conditions.

VI. EXPERIMENTAL RESULTS

The prototype system depicted in Fig. 15 has been constructed to assess the proposed system. The converter's output is managed using a 72 MHz ARM Cortex-M4 microcontroller, the STM32f407. Hall sensors are employed to measure phase currents. Additionally, a magnetic sensor strip with a resolution of 10 μm is positioned alongside the stator to acquire displacement and speed signals. The microcontroller's internal timer serves as a capture channel for these signals. All the collected signals are stored in the

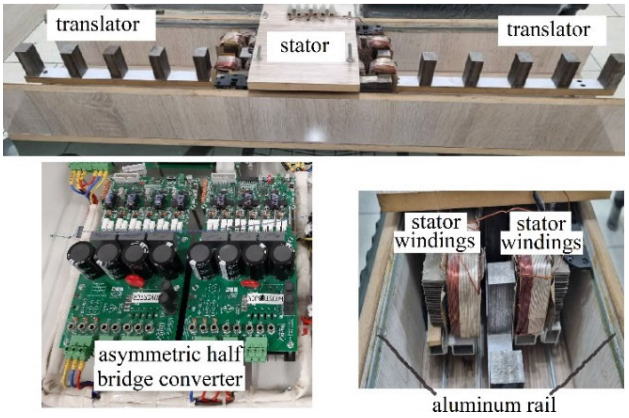

FIGURE 15. Prototype system including the proposed LSRM.

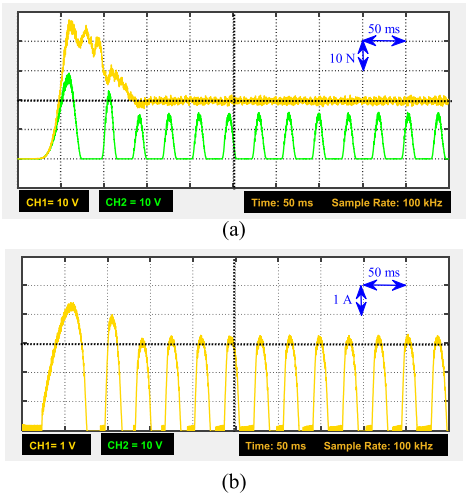

FIGURE 16. Measured data in prototype system, (a) force, (b) current.

microcontroller's external memory at intervals of 10 ms, and they are accessed from there. Consequently, due to this synchronization, instantaneous parameter sampling data, in line with the control loop time (1 ms), does not find representation in the experimental outcomes. As a result, the stored experimental data are transferred to the software for the purpose of plotting curves.

The proposed control system has been applied to the prototype motor, and its performance has been evaluated. To demonstrate the efficacy of the proposed system, its performance has been compared at different speeds using the methodology presented in [14]. The total propulsion force and phase force curves are depicted in Fig. 16, while the current waveform of one of the phases is also provided. These curves have been obtained by utilizing the data stored in the external memory of the microcontroller and connecting it to the software.

The propulsion force curves within a limited range have been compared for two methods at two different speeds, as illustrated in Fig. 17. According to these plots, the two control methods exhibit relatively similar performance at a speed of 0.5 m/s, whereas at higher speeds like 2 m/s, the

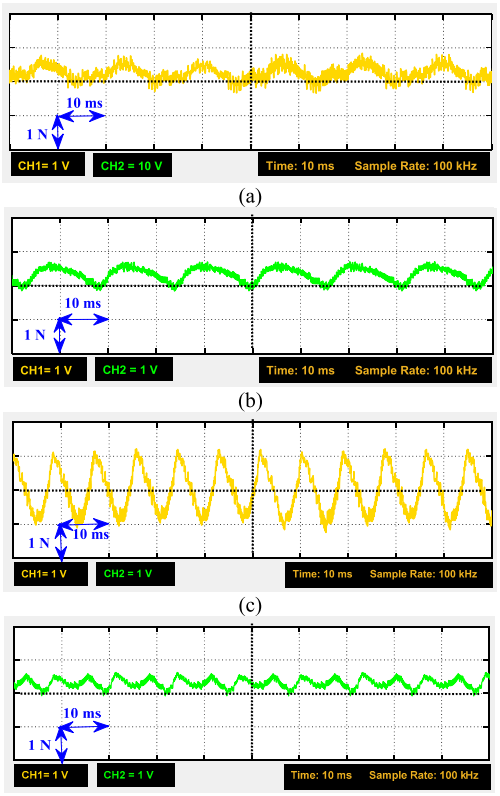

FIGURE 17. Measured force comparison, (a) controller in [14], 0.5 m/s, (b) Proposed controller, 0.5 m/s, (c) controller in [14], 2 m/s, (d) proposed method, 2 m/s.

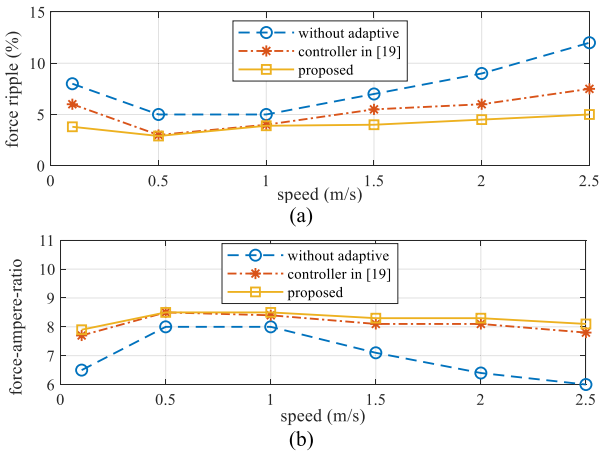

FIGURE 18. Performance comparison between three methods, (a) force ripple, (b) force-ampere-ratio.

proposed system outperforms and demonstrates lower ripple. The comparison of ripple levels as well as the force-ampere ratio for different speeds can be observed in Fig. 18.

Numerical data including the average, maximum, and ripple values for force curves in Fig. 17 are shown in TABLE 3.

In Fig. 18, the results obtained from the proposed method without adaptive turn on calculator, the approach presented in [14], and the proposed strategy are depicted together. These results confirm the improved performance of the proposed control system across a broader range of speeds.

VII. CONCLUSION

A modern structure framework for a linear switched reluctance motor with simultaneous three phase excitation capability was presented in this paper. The structure doesn't require changing the motor's dimensions; instead, it comes from arranging different parts of the motor together in a special way. The proposed arrangement led to improved force distribution and quality as well as enhanced reliability of the drive system. A novel control method, combining a switching table and current control techniques, shows its effectiveness through the utilization of a 12 voltage vectors switching table for motor phase current control. The integration of an adaptive control system, facilitating online calculation of the turn-on position, enhanced the system's adaptability across varying speeds. Both simulation results and practical experimental tests unequivocally validate the proposed technique and its performance superiority in comparison to conventional approaches.

ACKNOWLEDGMENT

The findings achieved herein are solely the responsibility of the authors.

REFERENCES

[1] N. Prasad, S. Jain, and S. Gupta, "Review of linear switched reluctance motor designs for linear propulsion applications," *CES Trans. Electr. Mach. Syst.*, vol. 6, no. 2, pp. 179–187, Jun. 2022.

[2] N. S. Lobo, H. Sun Lim, and R. Krishnan, "Comparison of linear switched reluctance machines for vertical propulsion application: Analysis, design, and experimental correlation," *IEEE Trans. Ind. Appl.*, vol. 44, no. 4, pp. 1134–1142, Aug. 2008.

[3] R. Cao, E. Su, and M. Lu, "Comparative study of permanent magnet assisted linear switched reluctance motor and linear flux switching permanent magnet motor for railway transportation," *IEEE Trans. Appl. Supercond.*, vol. 30, no. 4, pp. 1–5, Jun. 2020.

[4] D. Wang, X. Wang, and X.-F. Du, "Design and comparison of a high force density dual-side linear switched reluctance motor for long rail propulsion application with low cost," *IEEE Trans. Magn.*, vol. 53, no. 6, pp. 1–4, Jun. 2017.

[5] M. Lu and R. Cao, "Comparative investigation of high temperature superconducting linear flux-switching motor and high temperature superconducting linear switched reluctance motor for urban railway transit," *IEEE Trans. Appl. Supercond.*, vol. 31, no. 5, pp. 1–5, Aug. 2021.

[6] M. Vatani and M. Mirsalim, "The modular and crooked-tooth translator linear switched reluctance motor with a high-thrust per weight," *IEEE Trans. Transport. Electrific.*, vol. 7, no. 3, pp. 1359–1369, Sep. 2021.

[7] H.-J. Liang, S.-D. Huang, G.-Z. Cao, and T. Liang, "Design and analysis of a large-thrust and small-deformation double-sided linear switched reluctance motor," in *Proc. IEEE 5th Int. Electr. Energy Conf. (CIEEC)*, May 2022, pp. 2029–2034.

[8] M. R. Soltanpour, H. Abdollahi, and S. Masoudi, "Optimisation of double-sided linear switched reluctance motor for mass and force ripple minimisation," *IET Sci., Meas. Technol.*, vol. 13, no. 4, pp. 509–517, Jun. 2019.

[9] J. Rodriguez et al., "Latest advances of model predictive control in electrical drives—Part II: Applications and benchmarking with classical control methods," *IEEE Trans. Power Electron.*, vol. 37, no. 5, pp. 5047–5061, May 2022.

[10] S. Masoudi and H. Mehrjerdi, "A multilayer perception trained method in speed control of a linear switched reluctance motor," *IEEE Trans. Power Electron.*, vol. 37, no. 4, pp. 4475–4483, Apr. 2022.

[11] S. Masoudi, H. Mehrjerdi, and A. Ghorbani, "Adaptive control strategy for velocity control of a linear switched reluctance motor," *IET Electr. Power Appl.*, vol. 14, no. 8, pp. 1496–1503, Aug. 2020.

[12] J. Cai and Z. Deng, "Unbalanced phase inductance adaptable rotor position sensorless scheme for switched reluctance motor," *IEEE Trans. Power Electron.*, vol. 33, no. 5, pp. 4285–4292, May 2018.

[13] G. Fang, J. Ye, D. Xiao, Z. Xia, X. Wang, and A. Emadi, "Time-efficient torque shaping for switched reluctance machines from linear space," *IEEE Trans. Power Electron.*, vol. 36, no. 8, pp. 9361–9371, Aug. 2021.

[14] N. Yan, X. Cao, and Z. Deng, "Direct torque control for switched reluctance motor to obtain high torque-ampere ratio," *IEEE Trans. Ind. Electron.*, vol. 66, no. 7, pp. 5144–5152, Jul. 2019.

[15] L. Feng, X. Sun, X. Tian, and K. Diao, "Direct torque control with variable flux for an SRM based on hybrid optimization algorithm," *IEEE Trans. Power Electron.*, vol. 37, no. 6, pp. 6688–6697, Jun. 2022.

[16] T. Zhu, X. Cao, Q. Yu, Z. Deng, and Z. Hao, "Direct torque control with phase commutation optimization for single-winding bearingless switched reluctance motor," *IEEE Trans. Power Electron.*, vol. 37, no. 11, pp. 13238–13249, Nov. 2022.

[17] W. Li, Z. Cui, S. Ding, F. Chen, and Y. Guo, "Model predictive direct torque control of switched reluctance motors for low-speed operation," *IEEE Trans. Energy Convers.*, vol. 37, no. 2, pp. 1406–1415, Jun. 2022.

[18] D. Ronanki, K. R. Pittam, A. Dekka, P. Perumal, and A. R. Beig, "Phase current reconstruction method with an improved direct torque control of SRM drive for electric transportation applications," *IEEE Trans. Ind. Appl.*, vol. 58, no. 6, pp. 7648–7657, Nov. 2022.

[19] P. Ren, J. Zhu, Z. Jing, Z. Guo, and A. Xu, "Improved DITC strategy of switched reluctance motor based on adaptive turn-on angle TSF," in *Proc. 5th Int. Conf. Elect. Eng. Green Energy*, Berlin, Germany, 2022, pp. 8–11.

[20] S. Xu, L. Tao, G. Han, and C. Liu, "A novel driven scheme regarding to current dynamics enhancement for switched reluctance motor system," *IEEE Trans. Transport. Electrific.*, vol. 9, no. 3, pp. 4447–4457, Sep. 2023.

SIAMAK MASOUDI (Member, IEEE) received the B.Sc. degree in power engineering from Tarbiat Moallem University, Tabriz, Iran, in 2006, and the M.Sc. and Ph.D. degrees in electrical machines and drives from the University of Tabriz, Tabriz, in 2009 and 2016, respectively. Since 2010, he has been a member of Science with Azad University, Abhar Branch, Zanjan, Iran. Since 2022, he has been a Researcher with the Engineering Faculty, Qatar University, Doha, Qatar. His current research interests include electrical machines design and control and linear motors/generators.

LAZHAR BEN-BRAHIM (Life Senior Member, IEEE) received the B.Sc. and M.Sc. degrees in electrical engineering from the National School of Engineers of Tunis, Tunisia, in 1985 and 1987, respectively, and the Ph.D. degree in electrical engineering from Yokohama National University, Yokohama, Japan, in 1991. From 1991 to 1997, he was with Toshiba Corporation, where he was engaged in research and development of power electronics and motor drive systems. Since September 1997, he has been with the Industrial Technology Department, College of Technology, Qatar University. He was the Head of the Industrial Technology Department, from 1998 to 2005. In September 2005, he joined the Electrical Engineering Department, Qatar University. He was also the Industrial Electronics Chair of RasGas (QatarGas) Company and the Head of the Electrical Engineering Department. He invented several new techniques for use in motor drives, power electronics, and sensors. These inventions are registered in more than 12 international patents. His current research interests include power electronics, renewable energy, electric vehicles, electric drives, and sensor and instrumentation. He was an Associate Editor of the *Electrical Engineering* journal (Springer). He is an Editor of the *Electronics* journal (MDPI).

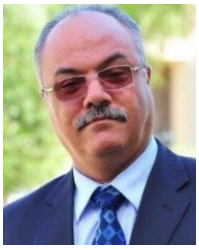

ADEL GASTLI (Senior Member, IEEE) received the B.Sc. degree in electrical engineering from the National School of Engineers of Tunis, Tunisia, in 1985, and the M.Sc. and Ph.D. degrees in electrical and computer engineering from Nagoya Institute of Technology, Japan, in March 1990 and March 1993, respectively. From September 1985 to September 1987, he was with the National Institute for Standards and Intellectual Property, Tunisia. He was with Mitsubishi Electric Corporation, Japan, from April 1993 to July 1995. He joined the Electrical and Computer Engineering Department, Sultan Qaboos University, Oman, in August 1995. He was the Head of the Department, from September 2001 to August 2003 and from September 2007 to August 2009. He was appointed as the Director of the Sultan Qaboos University Quality Assurance Office, from February 2010 to January 2013. In February 2013, he joined the Electrical Engineering Department, Qatar University, as a Professor and the Kahramaa-Siemens Chair of Energy Efficiency. From August 2013 to September 2015, he was appointed the College of Engineering Associate Dean for Academic Affairs. He is currently a Professor with the Electrical Engineering Department and a Senior Assessment and an Evaluation Specialist with the Academic Planning and Quality Assurance (APQA) Office, Qatar University. His current research interests include power electronics and electric drives, energy efficiency, renewable energy, electric vehicles, and smart grids.

NASSER AL-EMADI (Member, IEEE) received the B.Sc. and M.Sc. degrees in electrical engineering from Western Michigan University, Kalamazoo, USA, in 1989 and 1994, respectively, and the Ph.D. degree in power system from Michigan State University, East Lansing, MI, USA, in 2000. He is currently the Assistant Vice President of Faculty Affairs, Qatar University, and an Associate Professor with the Department of Electrical Engineering, Qatar University, Doha, Qatar. He has a wide experience in electric power systems, control, protection, and sensor interfacing, control of multiphase motor drives, renewable energy sources, and the integration of smart grid. He is a Founding Member of Qatar Society of Engineers and a member of the Advisory Board of the IEEE Qatar Section.

MOHAMED DJEMAI (Senior Member, IEEE) received the master's degree in electrical engineering from École Nationale Polytechnique of Algiers, Algeria, in 1991, and the Ph.D. degree in control engineering from the University of Paris XI, CNRS-LSS, France, in 1996.

He has been a Full Professor with the University of Valenciennes and Hainaut-Cambresis, Valenciennes, France, since 2008. He is currently with the Laboratory of Industrial and Human Automation, Mechanics and Computer Science, CNRS, UMR 8201. He is a member of IFAC TC 2.1 Control System and IFAC TC. 1.3 on Discrete Event and Hybrid Systems. He was a Visiting Professor with Northumbria University, in 2010 and 2013. His research interests include nonlinear control, observation, and fault detection theory, including hybrid system control, sliding-mode, and variable structure systems, with applications to power systems, robots, and vehicles.